Surfaces and Interfaces 23 (2021) 100989

Contents lists available at ScienceDirect

Surfaces and Interfaces

journal homepage: www.sciencedirect.com/journal/surfaces-and-interfaces

Silicon Dioxide Deposited Using Atmospheric Pressure Plasma Chemical Vapor Deposition for Improved Adhesion and Water Intrusion Resistance for Lightweight Manufacturing

Zachary Jeckell [a], Dhruval Patel [a], Andrew Herschberg [a], Tag Choi [a], David Barlaz [a], Lucia Bonova [a,c], Ivan Shchelkanov [b], Brian Jurczyk [b], David Ruzic [b]

[a] Department of Nuclear, Radiological, and Plasma Engineering, University of Illinois at Urbana-Champaign, 201 S Goodwin Ave, Urbana, IL 61802
[b] Starfire Industries 2109 S Oak St, Champaign, IL 61820
[c] Advanced Technologies Research Institute, Faculty of Materials Science and Technology in Trnava, Slovak University of Technology in Bratislava, Jána Bottu 25, 91724 Trnava, Slovakia

ARTICLE INFO

Keywords:
Atmospheric pressure plasma
chemical vapor deposition
silicon oxide
lap shear strength
barrier coating

ABSTRACT

This work aims to demonstrate the barrier coating, and adhesion promoting properties of silica-based coatings deposited using an atmospheric pressure plasma torch (APPT). This is achieved by applying an industrial grade adhesive to silica thin films deposited, on the surfaces to be joined, using atmospheric pressure plasma chemical vapor deposition (APP-CVD), to make single joint lap shear samples of different metal combinations commonly found in lightweight manufacturing, such as aluminum and magnesium as well as steel. To deposit these thin films, two separate silicon based organic precursors, hexamethyldisiloxane (HMDSO), and tetraehylorthosilicate (TEOS), are used. Samples are bonded using DuPont Betamate 1486 adhesive, and the lap shear results for these films are compared to the lap shear results of a chemically cleaned control using the same adhesive. The APPT uses a microwave power supply and gas mixtures of N_2 and Ar. The adhesion of the films are tested using lap shear, and elevated temperature water soaks are conducted on the joints as well to simulate environmental exposure. Lap shear results, from samples with silica thin films, have an increase of max shear stress of 25%-115% compared to control samples depending on material. After exposure to water soak the max shear strength of the joints decreased by less than 15%, which demonstrates the films capabilities as a water barrier. Film morphology is examined using Scanning Electron Microscopy (SEM), and the film's composition and approximate thickness are obtained using Rutherford Backscattering Spectroscopy (RBS).

1. Introduction

As the automotive industry shifts towards lightweight manufacturing there is a need for a cost-effective method to bond dissimilar metals commonly used in manufacturing, such as aluminum and magnesium. For this reason, the automotive industry is looking for methods that improve the performance of dissimilar metal joints bonded using adhesives. The primary method for this procedure was, until recently, the Alodine dip coating process, an dipping process where entire parts are submerged in a solution to clean and deposit a conversion coating [1]. The Alodine treatment coats the entire part, when typically only small joints require the coating. This process is inherently wasteful, and because this is typically done off site it adds transportation costs and creates chemical waste which can both endanger workers and incurs costly disposal [1]. A newer technique to improve adhesion involves using a laser which roughens and cleans the surface, as well as removes the native oxide [2–4].

Silicon dioxide thin films are versatile and offer many potential advantages for lightweight manufacturing. Significant research has been published on the oxygen and water barrier properties of silicon dioxide thin films, which is of great interest for the food packing and medical industries [5–8]. Thin silicon dioxide films have been demonstrated to improve the barrier and corrosion resistance of various materials including aluminum [9], steel [10], magnesium [11–13], and even carbon fiber reinforced polymers [6–8,14–18] . Research has also been done that highlights silica thin films for their ability to act as an

Abbreviations: APPT, Atomospheric pressure plasma torch; APP-CVD, atmospheric pressure plasma chemical vapor deposition; HMDSO, hexamethyldisiloxane; TEOS, tetraethylorthosilicate; RBS, Rutherford Back Scattering.

https://doi.org/10.1016/j.surfin.2021.100989
Received 10 December 2020; Received in revised form 21 January 2021; Accepted 30 January 2021
Available online 4 February 2021

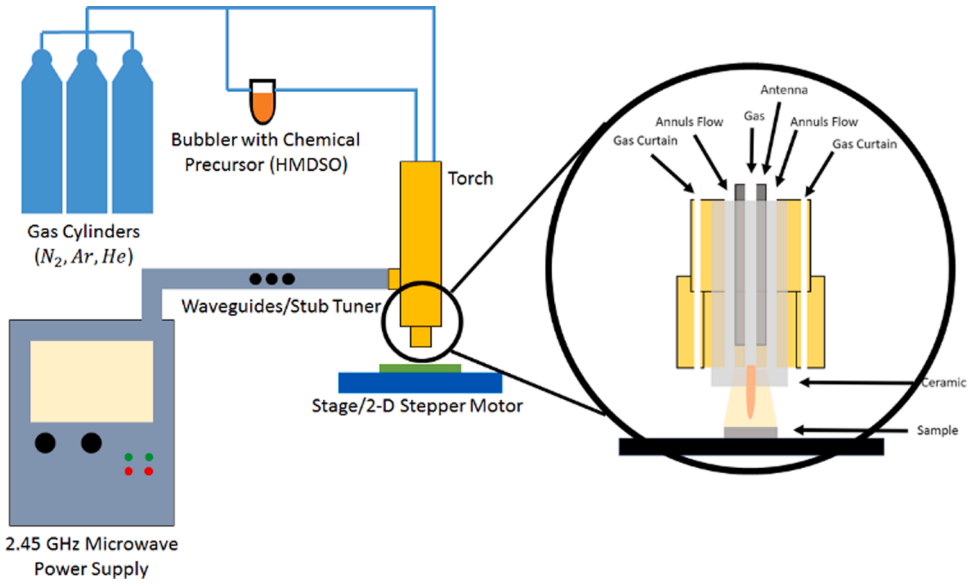

Fig. 1. Experimental schematic demonstrating how microwaves propagate from the power supply to the torch through a series of waveguides. The plasma is matched using a series of stub tuners. Gas and precursor delivery from the wicking bulb is also shown. An exploded view of the torch highlights the torch design that allows for three distinct regions of gas flow.

adhesion promoter by improving epoxy bond strength [19]. The combination of improved adhesion and environmental barrier performance made it a strong candidate for automotive applications.

Silicon dioxide coatings may be deposited in numerous ways. The sol-gel method was one of the first large scale techniques for depositing silicon dioxide with acceptable barrier properties, however, it has been shown to have poor substrate adhesion. The drying process can lead to shrinkage and induce stress in the films that can lead to cracks that serve as corrosion pathways [1,12,20] .The highest quality silicon dioxide films are deposited using low pressure vacuum systems, however this technique requires processing *in vacuo* which increases cost and hinders scalability [7,15,17,21].

Atmospheric pressure plasmas offer a tradeoff that improves throughput and enables point of manufacturing deposition at the cost of film quality. Several different atmospheric pressure plasma sources, such as dielectric barrier discharges [13,18,21,22], atmospheric pressure plasma jets [8,19,23,24], as well as RF [25,26] and microwave torches [25], have had success depositing high-quality silicon dioxide on a wide variety of substrates. Evaporative and laser assisted methods have also been used to deposit metal oxide coatings at atmospheric pressure, such as yitria stabilized zirconia and aluminum oxide, but the temperatures required for metal evaporation limit the types of substrates that can be used [27,28]. Additionally, plasma sources offer an additional advantage in plasma cleaning. Plasma cleaning has been well studied for its ability to clean surfaces, and increase surface wettability typically by activating the surface [29–33]. Plasma cleaning has also been shown to improve the shear strength of adhesives applied to polymers and other surfaces that were plasma cleaned [2,34–38]. Several processes, including the deposition of conversion coatings, rely on these types of processes as a pristine active surface is required for the pretreatment layer which must be well adhered so that the corrosion protection primer can be applied [1].

This work highlights a process for depositing silicon dioxide coatings using an APPT operating using a 2.45 GHz microwave power supply. The goal of this research is to demonstrate how silicon dioxide thin films with sub 100 nm thickness deposited on a material can improve the strength of single joint lap shear bonds, and that these coating hold up to environmental conditions adequately.

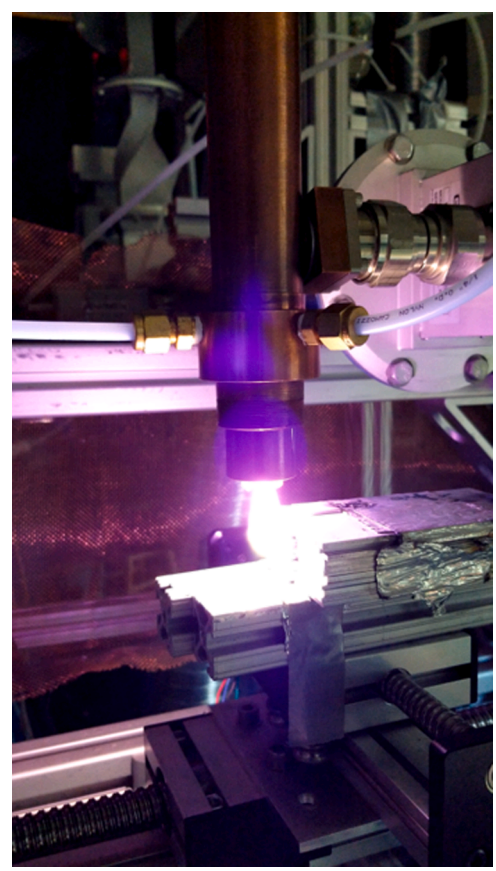

Fig. 2. Image of APPT used for processing samples, as well as stepper motor and sample stage

2. Materials and methods

2.1. Experimental setup

Silicon-based coatings were deposited using an APPT. The APPT is

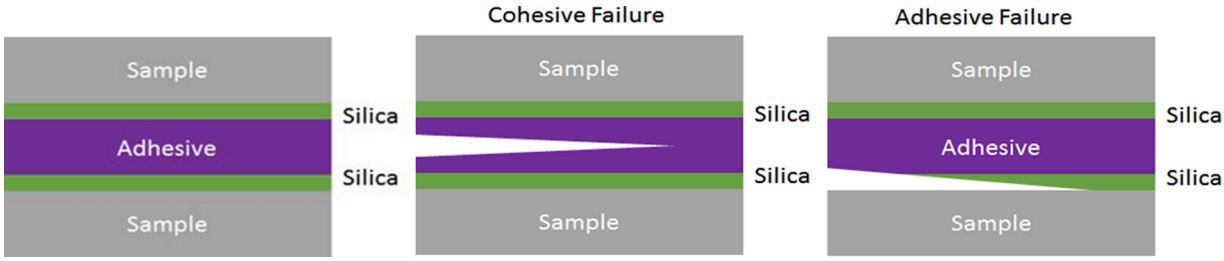

Fig. 3. Single lap shear joint schematic, and illustration of two common failure mechanisms

comprised of two concentric electrodes, between which the microwaves propagate. The 0.25" outer diameter hollow titanium antenna is used as the inner electrode, and the outer electrode is the copper body of the torch which has an inner diameter of 5/8". A schematic for the experimental setup, with an exploded view, is shown in Figure 1. Torch operation is shown in Figure 2.

The Cober S6F Industrial Microwave Generator, a 6 kW power supply, is used to excite 2.45 GHz microwaves. The microwaves propagate through a series of waveguides which connect to a 7/16" DIN connector that is attached to the side of the torch. To match the plasma such that reflected power is less than 5%, a series of four stub tuners is used to shift the microwaves. The forward and reflected power are measured using two microwave power sensors (Mini-Circuits PWR-SEN-6G+). Additionally, the position of the inner electrode, which is the hollow titanium antenna, and end-wall of the torch, can be positioned to change the operating frequency of the torch from 900 MHz to 2.45 GHz. This is possible because the end-wall of the torch acts as the systems ground, and the tip of the antenna is the high field point.

The torch was designed to have three distinct regions of gas flow. The antenna used for this setup is hollow, which allows for gas flown through it, this is typically where precursors and their carrier gasses are flown. The next region of flow is known as the annulus flow, which is channel that most of the processing gas flows through. The gas curtain allows for isolation of the reaction zone from outside contamination.

2.2. Experimental parameters

Two stepper motors are used for motion under the torch in an x-y plane, that enables processing of large area surfaces, with translational speeds ranging up to 30 mm/s. The typical processing pattern used for these experiments is a series of horizontal passes that go across the entire set of samples, which are separated by steps down the length of the samples.

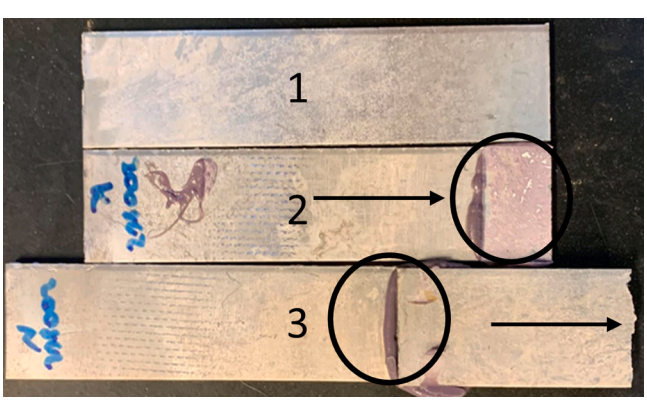

Fig. 4. Three separate samples, the first being an untreated cast Mg coupon, the second being an example of cohesive failure, and the third being a rare failure mechanism in which the metal breaks before the adhesive. The arrow indicates the area where failure occurred, and the circle indicates the area where the adhesive is applied.

The processing gasses composition and flow rate are perhaps the most important experimental parameters. Typical gas flow rates used on are between 10 and 30 liters per minute (lpm). The microwave torch used in this experiment can operate with helium (Airgas UHP), argon (Airgas UHP), nitrogen (Airgas UHP), and air (Airgas Industrial), as well as various combinations of these gasses. The microwave powers used for these experiments were varied between 400-800 W.

The ability to plasma preclean before deposition was another experimental parameter, as substrates were treated as received and cast materials were contaminated with residual mold release. Previous experiments performed on this APPT demonstrated significant removal of such contaminations [29]. However, plasma precleaning requires an additional processing steps, so processing conditions were found that allowed for plasma cleaning to occur at the same time as deposition by utilizing the antenna and annular regions of gas flow.

For this investigation, two separate precursors, hexamethyldisiloxane (HMDSO) [7,8,17,18,21,22,24,39] and tetraethylorthosilicate (TEOS) [11,13,17,23,26] were studied because of the numerous publications using them, and their relative performances were compared to each other and the industrial benchmark. Both are delivered using a wicking chamber with N_2 carrier gas of flow rates of 0.2 lpm set by a mass flow controller, which corresponds to roughly 0.025 mL/min for HMDSO and 0.002 mL/min for TEOS. This is a large disparity, however, attempts to lower flowrates for HMDSO below 0.025 mL/min had less consistency. Flow rates higher than this, specifically for HMDSO, led to increased film porosity and in many cases the formation of powder on the surface due to nucleation in the gas phase. In all cases, however, increasing carrier gas flow rate higher than 0.3 lpm N_2 led to poor performance.

2.3. Lap shear sample preparation and water soak procedure

To demonstrate the versatility of the deposition several different materials were tested. These materials are, 7003 aluminum extrusions, Aural 5 cast aluminum plates, AZ91D cast magnesium and 420LA steel. The coupons are 4 inches in length, 1 inch wide, and have a height between 2 and 3 mm depending on the material. Coupon roughness was typically 2-3 μm, or more than an order of magnitude greater than the expected SiO_2 film thicknesses. These coupons were placed on a 2-D stepper motor setup at a set distance beneath the APPT. Utilizing this setup, the top 1 inch by 1 inch of the coupons are treated such that a thin layer of silicon dioxide is deposited. After treatment, an industrial strength adhesive (DuPont Betamate 1486) is applied to the top half inch of one coupon in a pair. Silica spacer beads (Potters Industries Incorporated 0.00098") are then dispensed onto the adhesive to prevent adhesive from squeezing out. Next, the two samples are pressed and held together during the duration of the curing, which is a 35-minute cure time at a temperature of 180 ℃ in a convection oven.

To test the coatings efficiency as a water barrier, water soak tests are performed on single joint lap shear samples and compared to samples made under the same conditions that were not water soaked. Single joint lap shear samples were water soaked for a duration of 168 hours at an elevated temperature of 55 ℃. A pyrex dish was chosen to minimize metallic contaminations from the bath. After the 168-hour water soak is

finished, the materials lap strength is tested and compared to the non-water-soaked samples. If less than a 20% decrease in max strength is observed, the samples meet the benchmark set by the automotive industry.

2.4. Material characterization

2.4.1. Lap shear

The shear strength of the deposited films was determined using lap shear testing on a single joint. The 10 kN load cell was operated at a ramp speed of 0.08 mm/s, at room temperature, and were tested until failure.

Figure 3 shows what the coupon pair looks like after it is done curing. The failure mechanism of the adhesive is also reported because it correlates well to overall film quality and film coverage. While there are numerous failure mechanisms, the two that are highlighted in Figure 3 are cohesive failure and adhesive failure. Cohesive failure is characterized by failure within the adhesive, whereas adhesive failure is where the glue lifts off one of the samples. In the case of cohesive failure, the bond of the silica to the sample and the silica to the adhesive have larger shear strength than the adhesive has to itself, which implies that the film is well adhered. For the work presented in this paper, a sample is only adequate if it both passes the minimum stress benchmark of 19 MPa and has a cohesive or mostly cohesive failure mechanism both before and after water soak.

Figure 4 displays representative sample appearances before and after lap shear, including a failure mechanism in which the metal in one of the two samples fails before the adhesive, demonstrating the adhesive strength after deposition.

2.4.2. SEM

In addition to mechanical testing, cross sections of the films deposited by the two different precursors were observed using the HITACHI 4800 scanning electron microscope, by using a cleaved silicon wafer as the substrate. This was done to increase the speed and reduce the cost of examining the films microstructures, as well as offering a considerably smoother interface to ease the difficulty in imaging sub 100 nm thin films.

2.4.3. RBS

Additionally, RBS was used both to determine the composition of the deposited films as well as to roughly estimate film thickness. RBS was chosen primarily because of difficulties using other techniques such as ellipsometry or XPS due to the roughness of the substrate. The film thickness can be approximated by converting the output of atoms/cm^2 to cm by assuming a user defined density of the film in g/cm^3 and converting grams to atoms using Avogadro's number. For this analysis, the density of amorphous silicon dioxide was chosen to be 2.196 g/cm^3, which is an approximation because it assumes a density for the material that is without voids or porous structure. The RBS uses 2.024 MeV alpha particles, which are accelerated by the NEC pelletron at an angle of incidence of 22.50 degrees to the sample. Analysis of the spectrum was done using the SIMNRA software, which takes parameters, such as number of layers and their composition, and iterates to make an analytical spectrum that attempts to fit the experimental data. For this investigation, the substrates used were mirror polished Al 6061 alloy, which was chosen over other alloys due to the difficulty associated with fitting very rough metal coupons with alloys that contain higher concentration of alloying elements. Therefore, the second layer in SIMNRA was chosen to be the substrate, which for simplicity only aluminum, magnesium, and silicon were chosen in accordance with their alloy composition. The first layer was selected as 2 elements, silicon and oxygen, and was initialized with a Si/O ratio of 1:2. RBS analysis was performed on three separate films, and each film analysis was performed at three separate locations to gain an understanding of the uniformity of the film. Two of the three recipes were chosen to study the best results

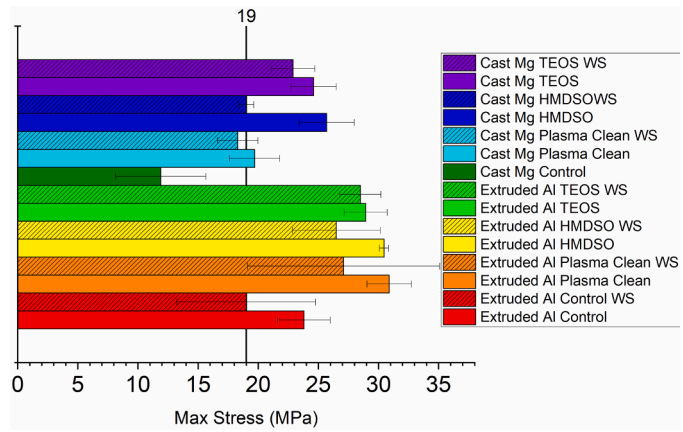

Fig. 5. Comparison of max shear stress for films deposited using HMDSO and TEOS as chemical precursors on cast Mg and Extruded Al for both water soaked (WS) and non-water soaked samples Each bar represents the average of 5 independent sample pairs and the error bars are +/- 1 standard deviation. Control samples have no pretreatment or cleaning. Plasma cleaned has sample plasma exposure as SiO_2 samples without precursor flow.

for HMDSO and TEOS, and because the TEOS film is thinner another recipe was performed that repeated the TEOS recipe five times over one sample to intentionally deposit a thicker film.

2.4.4. Handheld XRF

One of the primary challenges this process will face, is verification of APP-CVD silica deposition at point of manufacturer. For APP-CVD to be a viable alternative to current techniques there must be a quick, nondestructive testing method to ensure that the silica thin film, which is invisible to the naked eye, is deposited. X-ray fluorescence, or XRF, specifically a Niton XL5 handheld XRF with the coating thickness measurement package, satisfies the criteria and meets the constraints for such a challenge. By calibrating the XRF to alloys used in manufacturing, the XRF can do a fast single-element scan against the calibrated background to look for certain elements. For this work the XRF was calibrated for the AZ91D magnesium alloy and the 7003 Al alloy, and was scanning for silicon.

3. Results and discussion

As noted previously, the design of the torch offers a large parameter space, so it is important to understand how process optimization was done and how the processing parameters were narrowed down to the best scenarios. Early work concluded that gas mixtures of N_2 and argon totaling up to roughly 20 total liters per minute led to the best results, specifically, the combination of 17 lpm N_2 and 4 lpm Ar. Extruded aluminum was found to be the most tolerant material, likely due to its smoother interface and lack of mold release found on cast metals, so recipe optimization was first done on extruded aluminum. Through this process, the optimal conditions were found for all materials and relative process tolerances were observed. For instance, it was observed that microwave power and spacing between stepper motor paths to be variables with relatively large tolerances, whereas carrier gas flow rate has a much tighter tolerance due to nucleation in the gas phase and the subsequent formation of powder on the surface, a trend that other groups have similarly noticed [40].

3.1. HMDSO and TEOS comparison

3.1.1. HMDSO and TEOS lap shear comparison

This work aims to compare silica films deposited using two different precursors: HMDSO and TEOS. The performance of these films is quantified by their adhesion, and their ability to prevent water from

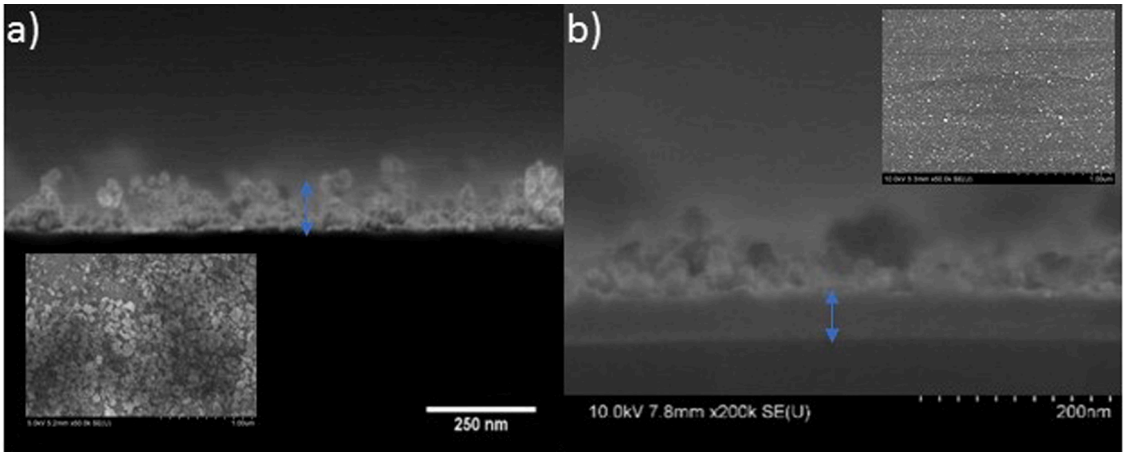

Fig. 6. SEM of Film deposited using (a) HMDSO as the chemical precursor with microwave power of 600 W, gas flow rate of 17 lpm N_2 4 lpm Ar and 0.2 lpm N_2 through the wicking chamber for 1 pass at 4 mm/s, (b) SEM of a film deposited using TEOS as a chemical precursor with microwave power of 600 W gas flow rate of 17 lpm N_2 4 lpm Ar and 0.2 lpm N_2 for ten passes at 4 mm/s. Blue arrows represent the measured film thickness performed in the ImageJ software. Inset images are top down SEM micrographs.

diffusing through to the substrate. Therefore, by comparing the maximum shear strength of joints treated with the two different precursors both before and after water soak, it is possible to determine which precursor is better suited for this application.

Examining Figure 5, it can be observed that the control for both cast Mg without water soak and extruded Al with water soak do not meet the adhesive's benchmark stress. While plasma cleaning improves joint strength above the benchmark after water soak for aluminum, performance variation, as seen in error bars, and consistency across materials in poor compared to SiO_2 treated coupons. When comparing the two precursors for extruded aluminum joints it appears as if the performance of the two precursors is comparable. However, when the material is cast Mg plates, it becomes clear that the films deposited using TEOS have better performance, particularly after water soak. Additionally, the HMDSO samples required a plasma preclean to ensure that the process is repeatable and that the films had the required adhesion, whereas films deposited with the best recipes using TEOS were able to utilize the three regions of flow on the torch to create a process that both cleans and deposits at the same time. This was done by delivering the precursor through the antenna, while all other processing gas was flown through the annulus. It is hypothesized that flowing the precursor through the antenna leads to a higher concentration locally near the center of the plume which may lead to the outer edges of the plasma to clean the surface before deposition. Attempts to do this using HMDSO as a precursor were unsuccessful, and still required a plasma preclean to have consistent cohesive failure. These results highlight silica's capabilities as both an adhesion promoter, but also a water intrusion barrier as the joints withstand water soak testing better than the controls.

3.1.2. HMDSO and TEOS morphology comparison

In order to understand the differences in performance of the two precursors, the morphologies of the films they produced were compared. This was done by depositing on a silicon wafer and cleaving in order to more quickly investigate the films without the need to do ion milling. In order to help with visualization these films were grown with processing times larger than used in the recipes shown. However, all other experimental parameters are the same as the ones used in processing.

When comparing Figure 6 (a) and (b) it is clear the two precursors produce films with drastically different morphologies and at significantly different deposition rates. The film produced by HMDSO has a thickness of 80 nm but was produced by 1 pass under the torch, whereas the TEOS film has a thickness of 70 nm but was deposited using 10 passes under the torch. TEOS was repeated 10 times for ease of viewing with the SEM. All lap shear samples created using TEOS as the chemical precursor were created using 1 pass. The morphology for Figure 6a appears to be full of dendritic structure with plenty of voids. Structures similar to this have been observed by another group [25] working with a microwave torch, which they attribute to the higher energy density than found in typical RF torches [25]. Comparing their morphology to the ones present in this work, the dendritic structures in their paper have larger radii. They hypothesize that increasing microwave power leads to an a decrease in the radii of the dendritic structures, which may be supported by this work [25]. The films deposited using TEOS, however, appear to have a dense layer with spherical structures on top. The dendritic structures, present most prominently in Figure 6a are believed to be caused by gas phase agglomeration of the precursor during transportation to the sample. Gas phase agglomeration, or nucleation in the gas phase is also commonly reported in literature [40]. If the flow rate of the precursor carrier gas is too high, the dendritic structures are poorly adhered which leads to a white power building up on the surface that can be easily wiped off. In contrast to the cross section images, both top down images show rough protrusions of different spacing and sizes. Based off the morphology differences it was hypothesized that while the dendritic structures present on samples coated with HMDSO may help to improve adhesion, due to an increased surface area for the adhesive to bond to, it may not function as well as a water intrusion barrier. The need for a functioning water barrier is important in corrosive environments, such as water baths of different materials, as it leads to faster degradation of the interface. For this reason, TEOS was a more suitable precursor.

3.1.3. HMDSO and TEOS RBS comparison

In addition to comparing the morphology, the composition and approximate thickness of the films were compared using RBS on mirror polished Al 6061 1 cm x 1cm samples. Figure 7 shows the overlay of the experimental RBS data with both the total simulated spectra, and the individual components.

Table 1 compares the three recipes based off atoms/cm^2 and their stoichiometry. It was observed that films deposited using TEOS as the chemical precursor had a stoichiometry closer to the expected Si/O ratio of 1:2. Additionally, due primarily to the difference in vapor pressure the atoms/cm^2 for the TEOS recipe are less than that of HMDSO, and since the conversion to thickness is a linear relationship this trend is also observed there. Due to the differences in porosity, however, one would expect to be the approximation for HMDSO film thickness to be more of an underestimate than the TEOS film thickness approximation Since the fits for the RBS data were adequate the surface roughness was not considered, which may contribute to increased inaccuracy in the

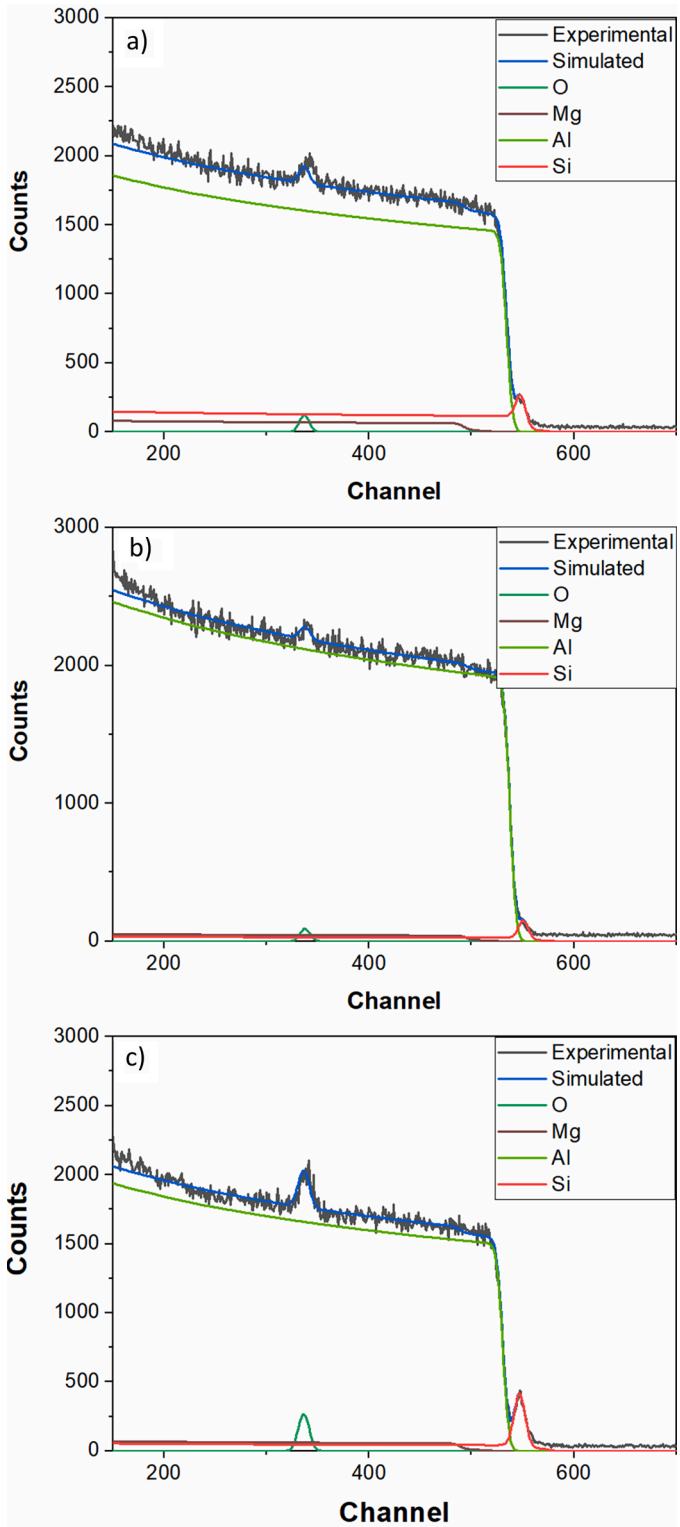

Fig. 7. Experimental and simulated RBS fitting of a silicon dioxide coating deposited using (a)HMDSO as the chemical precursor (b) TEOS as the chemical precursor, (c) Repeating the TEOS recipe 5 times on Al 6061 mirror polished samples

approximation. However, the data being fit as well as signifying that the surface roughness is not severe as the peaks are still relatively symmetric.

Table 1
Atoms/cm^2, approximate thickness and stoichiometry for three different recipes obtained using RBS. Error is +/- 1 standard deviation from three spots measured per sample. Recipes used are the HMDSO recipe with the highest average shear stress, the TEOS recipe with the highest average shear stress, and the TEOS recipe with the highest average shear stress repeated five times to intentionally deposit a thicker layer

Recipe	10^{15} Atoms/cm^2	Thickness (nm)	Measured Si/O Ratio
HMDSO	59.8 ± 6.87	27.2 ± 3.12	1/1.81
TEOS	41.0 ± 5.79	18.6 ± 2.63	1/2.02
TEOS 5x	158 ± 3.40	71.9 ± 1.54	1/1.96

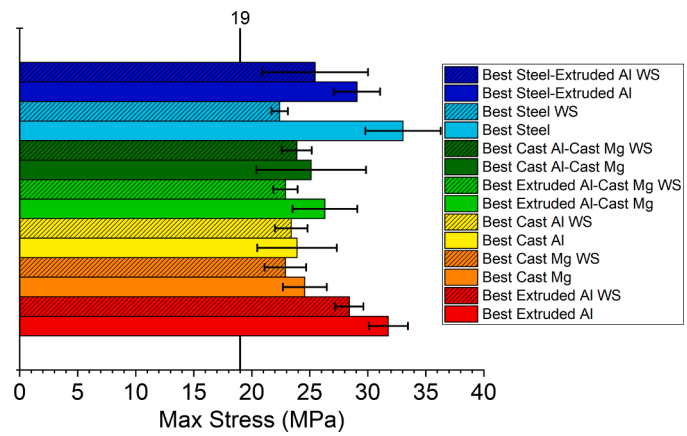

Fig. 8. Max shear stress results for the best recipe for each dissimilar metal combination, and their water soak results, which are denoted with WS. Each Bar represents the average of 5 independent sample pairs and the error bars are +/- 1 standard deviation

3.2. Bonding of dissimilar metals

For APP-CVD to be a viable option for lightweight manufacturing, it must demonstrate its capabilities to bond dissimilar metals together. Therefore, the versatility of this technique is demonstrated by performing lap shear on various metal-metal coupon pairs both before and after water soak. The presence of different metals in an elevated temperature water bath means that the thin film must operate both as a water barrier but also must be able to withstand the corrosive nature of the water bath. Figure 8 depicts the best results obtained for various metal joints using the techniques discussed in this paper. These best recipes all use TEOS as the precursor of choice, and overall have a total gas composition of 17 lpm N_2 and 4 lpm Argon with 0.2 lpm N_2 as the carrier gas through the TEOS wicking chamber. Microwave power between 400-800 W was used for all recipes and a substrate height of 7 mm was used for all materials except for steel, which had issues with blistering under the high temperature of the plasma jet. Steel was processed much further away at 20-24 mm.

Figure 8 shows that this technique is capable of bonding dissimilar metals with a max shear stress higher than that of the benchmark both before and after water soak. Therefore, the deposited thin films both improve adhesion and also are able to withstand the corrosive environment of the water soak testing, which highlights the films durability and water barrier properties.

3.3. Handheld XRF

A Niton XL5 Handheld XRF fast single element scan was used as a quick method to verify the deposition of silicon dioxide on our samples by identifying the presence of silicon as would be performed at point of manufacture. The XL5 requires a physical interlock switch to be depressed again the film before triggering and there were concerns that

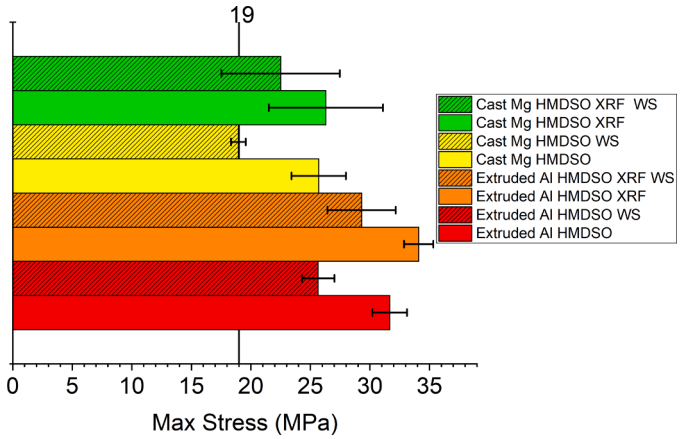

Fig 9. Max shear stress results for Cast Mg and Extruded Al samples and their water soaks (WS) with and without XRF testing before gluing. Each Bar represents the average of 5 independent sample pairs and the error bars are +/- 1 standard deviation

this process may scratch the films, or lead to a drop in performance. Therefore, to verify that the XRF was not inhibiting the performance of the film, lap shear and water soak lap shear were conducted on samples that were verified using the Niton. The recipe used for this test are the same HMDSO recipes discussed earlier. In each case, the film thicknesses are close to the instrument resolution so film thickness measurements were not considered reliable. The technique did consistently distinguish between treated and untreated samples. Figure 9 compares the results of the two cases, and their water soaks, and it was determined that the handheld XRF did not lead to damage of the film, and therefore is a valid way to verify film deposition at point of manufacturer.

4. Conclusion

This work demonstrates the capability and feasibility of thin silica films deposited using APP-CVD as adhesion and water barrier coatings for lightweight manufacturing. During recipe optimization, two separate silica precursors HMDSO and TEOS were tested and compared. It was observed that processes using HMDSO as the precursor required plasma precleaning to achieve cohesive failure, and that even then HMDSO films still struggled with dissimilar metal combinations. Processes using TEOS as the silicon precursor, however, produced films that led to cohesive failure without the need of plasma precleaning and was found to be much more tolerant to different material combinations. By examining the morphology of the two films, it was noted that the HMDSO films deposited using our process were porous and had dendritic structures whereas TEOS led to denser films. For this reason, we hypothesize that TEOS films function better as a water barrier than films deposited using HMDSO which is supported by the lap shear results. The film compositions were analyzed using RBS, and it was found that both chemical precursors were capable of depositing thin films with stoichiometry close to the desired silicon to oxygen ratio of 1:2, and without significant carbon incorporation. Recipe optimization took place for each dissimilar metal combination until cohesive failure and the benchmark criteria of 19 MPa was met for both non water soaked and water-soaked samples. Additionally, to address the issue of on-site processes verification, XRF was investigated as a potential solution. XRF has been demonstrated to both verify the presence of silicon, but also has been shown to not scratch or degrade the deposited film.

CREDIT

Zachary Jeckell: Methodology, Data Curation, Writing
Dhruval Patel: Data Curation
Andrew Herschberg: Data Curation, Formal analysis
Tag Choi: Data Curation
David Barlaz: Methodology, Writing - Review & Editing, Formal analysis
Lucia Bonova: Methodology, Supervision, Formal analysis
Ivan Shchelkanov: Methodology, Writing - Review & Editing, Supervision, Formal analysis
Brian Jurczyk: Methodology, Funding acquisition, Supervision, Formal analysis
David Ruzic: Funding acquisition, Writing - Review & Editing

Declaration of Competing Interest

The authors declare that they have no known competing financial interests or personal relationships that could have appeared to influence the work reported in this paper.

Acknowledgments

RBS and SEM analysis were carried out at the Materials Research Laboratory Central Research Facilities, University of Illinois. Lap shear testing was carried out in part in the Advanced Materials Testing and Evaluation Laboratory, University of Illinois. Thanks to Dr. Peter Kurath for assistance with lap shear. Thanks to Blair Carlson at General Motors for many fruitful discussions.

Funding: This work was supported by the Office of Energy Efficiency and Renewable Energy [DE-EE0008319]

References

[1] R.L. Twite, G.P. Bierwagen, Review of alternatives to chromate for corrosion protection of aluminum aerospace alloys, Prog. Org. Coatings. 33 (1998) 91–100, https://doi.org/10.1016/S0300-9440(98)00015-0.
[2] C. Mandolfino, E. Lertora, S. Genna, C. Leone, C. Gambaro, Effect of laser and plasma surface cleaning on mechanical properties of adhesive bonded joints, Procedia CIRP 33 (2015) 458–463, https://doi.org/10.1016/j.procir.2015.06.054.
[3] E.G. Baburaj, D. Starikov, J. Evans, G.A. Shafeev, A. Bensaoula, Enhancement of adhesive joint strength by laser surface modification, Int. J. Adhes. Adhes. 27 (2007) 268–276, https://doi.org/10.1016/j.ijadhadh.2006.05.004.
[4] A. Kurtovic, E. Brandl, T. Mertens, H.J. Maier, Laser induced surface nanostructuring of Ti-6Al-4V for adhesive bonding, Int. J. Adhes. Adhes. 45 (2013) 112–117, https://doi.org/10.1016/j.ijadhadh.2013.05.004.
[5] Y. Leterrier, Durability of nanosized oxygen-barrier coatings on polymers, Prog. Mater. Sci. 48 (2003) 1–55, https://doi.org/10.1016/S0079-6425(02)00002-6.
[6] S.R. Kim, M.H. Choudhury, W.H. Kim, G.H. Kim, Effects of argon and oxygen flow rate on water vapor barrier properties of silicon oxide coatings deposited on polyethylene terephthalate by plasma enhanced chemical vapor deposition, Thin Solid Films 518 (2010) 1929–1934, https://doi.org/10.1016/j.tsf.2009.07.147.
[7] D. Framil, M. Van Gompel, F. Bourgeois, I. Furno, Y. Leterrier, The Influence of Microstructure on Nanomechanical and Diffusion Barrier Properties of Thin PECVD SiOx Films Deposited on Parylene C Substrates, Front. Mater. 6 (2019) 1–10, https://doi.org/10.3389/fmats.2019.00319.
[8] H. Zhang, Z. Guo, Q. Chen, X. Wang, Z. Wang, Z. Liu, Deposition of silicon oxide coatings by atmospheric pressure plasma jet for oxygen diffusion barrier applications, Thin Solid Films 615 (2016) 63–68, https://doi.org/10.1016/j.tsf.2016.06.042.
[9] M. Abuín, A. Serrano, J. Llopis, M.A. García, N. Carmona, Silica doped with lanthanum sol-gel thin films for corrosion protection, Thin Solid Films 520 (2012) 5267–5271, https://doi.org/10.1016/j.tsf.2012.03.046.
[10] A. Delimi, Y. Coffinier, B. Talhi, R. Boukherroub, S. Szunerits, Investigation of the corrosion protection of SiOx-like oxide films deposited by plasma-enhanced chemical vapor deposition onto carbon steel, Electrochim. Acta. 55 (2010) 8921–8927, https://doi.org/10.1016/j.electacta.2010.08.008.
[11] Y.L. Kuo, K.H. Chang, C. Chiu, Carbon-free SiOx ultrathin film using atmospheric pressure plasma jet for enhancing the corrosion resistance of magnesium alloys, Vacuum 146 (2017) 8–10, https://doi.org/10.1016/j.vacuum.2017.09.028.
[12] J. Hu, Q. Li, X. Zhong, W. Kang, Novel anti-corrosion silicon dioxide coating prepared by sol-gel method for AZ91D magnesium alloy, Prog. Org. Coatings. 63 (2008) 13–17, https://doi.org/10.1016/j.porgcoat.2008.03.003.
[13] Y.L. Kuo, K.H. Chang, Atmospheric pressure plasma enhanced chemical vapor deposition of SiOx films for improved corrosion resistant properties of AZ31 magnesium alloys, Surf. Coatings Technol. 283 (2015) 194–200, https://doi.org/10.1016/j.surfcoat.2015.11.004.
[14] A. Bieder, A. Gruniger, P.R. von Rohr, Deposition of SiOx diffusion barriers on flexible packaging materials by PECVD, Surf. Coatings Technol. 200 (2005) 928–931, https://doi.org/10.1016/j.surfcoat.2005.02.004.

[15] T.N. Chen, D.S. Wuu, C.C. Wu, C.C. Chiang, Y.P. Chen, R.H. Horng, High-Performance Transparent Barrier Films of SiO[sub x]/SiN[sub x] Stacks on Flexible Polymer Substrates, J. Electrochem. Soc. 153 (2006) F244, https://doi.org/10.1149/1.2335592.
[16] D.G. Howells, B.M. Henry, J. Madocks, H.E. Assender, High quality plasma enhanced chemical vapour deposited silicon oxide gas barrier coatings on polyester films, Thin Solid Films 516 (2008) 3081–3088, https://doi.org/10.1016/j.tsf.2007.11.017.
[17] A.M. Coclite, A. Milella, R. d'Agostino, F. Palumbo, On the relationship between the structure and the barrier performance of plasma deposited silicon dioxide-like films, Surf. Coatings Technol. 204 (2010) 4012–4017, https://doi.org/10.1016/j.surfcoat.2010.05.024.
[18] N. Li, Y.L. Wu, J. Hong, I.A. Shchelkanov, D.N. Ruzic, SiOx Deposition on Polypropylene-Coated Paper With a Dielectric Barrier Discharge at Atmospheric Pressure, IEEE Trans. Plasma Sci. 43 (2015) 3205–3210, https://doi.org/10.1109/TPS.2015.2459720.
[19] M. Mokter Hossain, Q.H. Trinh, M.S.P. Sudhakaran, L. Sultana, Y.S. Mok, Improvement of mechanical strength of hydrophobic coating on glass surfaces by an atmospheric pressure plasma jet, Surf. Coatings Technol. 357 (2019) 12–22, https://doi.org/10.1016/j.surfcoat.2018.09.071.
[20] M. Guglielmi, Sol-Gel Coatings on Metals, J. Sol-Gel Sci. Technol. 8 (1997) 443–449, https://doi.org/10.1007/BF02436880.
[21] R.A. Siliprandi, S. Zanini, E. Grimoldi, F.S. Fumagalli, R. Barni, C. Riccardi, Atmospheric pressure plasma discharge for polysiloxane thin films deposition and comparison with low pressure process, Plasma Chem. Plasma Process. 31 (2011) 353–372, https://doi.org/10.1007/s11090-011-9286-3.
[22] R. Morent, N. De Geyter, S. Van Vlierberghe, P. Dubruel, C. Leys, E. Schacht, Organic-inorganic behaviour of HMDSO films plasma-polymerized at atmospheric pressure, Surf. Coatings Technol 203 (2009) 1366–1372, https://doi.org/10.1016/j.surfcoat.2008.11.008.
[23] C. Huang, C.H. Liu, C.H. Su, W.T. Hsu, S.Y. Wu, Investigation of atmospheric-pressure plasma deposited SiOx films on polymeric substrates, Thin Solid Films 517 (2009) 5141–5145, https://doi.org/10.1016/j.tsf.2009.03.054.
[24] R. Reuter, D. Ellerweg, A. Von Keudell, J. Benedikt, Surface reactions as carbon removal mechanism in deposition of silicon dioxide films at atmospheric pressure, Appl. Phys. Lett. 98 (2011) 1–4, https://doi.org/10.1063/1.3565965.
[25] J. Schäfer, J. Hnilica, J. Šperka, A. Quade, V. Kudrle, R. Foest, J. Vodák, L. Zajíčková, Tetrakis(trimethylsilyloxy)silane for nanostructured SiO2-like films deposited by PECVD at atmospheric pressure, Surf. Coatings Technol. 295 (2016) 112–118, https://doi.org/10.1016/j.surfcoat.2015.09.047.
[26] D. Lee, S. Yang, Surface modification of PDMS by atmospheric-pressure plasma-enhanced chemical vapor deposition and analysis of long-lasting surface hydrophilicity, Sensors Actuators, B Chem 162 (2012) 425–434, https://doi.org/10.1016/j.snb.2011.12.017.
[27] Y.L. Wu, J. Hong, D. Peterson, J. Zhou, T.S. Cho, D.N. Ruzic, Deposition of aluminum oxide by evaporative coating at atmospheric pressure (ECAP), Surf. Coatings Technol. 237 (2013) 369–378, https://doi.org/10.1016/j.surfcoat.2013.06.043.
[28] Z. Ouyang, L. Meng, P. Raman, T.S. Cho, D.N. Ruzic, Laser-assisted plasma coating at atmospheric pressure: Production of yttria-stabilized zirconia thermal barriers, J. Phys. D. Appl. Phys. (2011) 44, https://doi.org/10.1088/0022-3727/44/26/265202.
[29] L. Bónová, W. Zhu, D.K. Patel, D.V. Krogstad, D.N. Ruzic, Atmospheric pressure microwave plasma for aluminum surface cleaning, J. Vac. Sci. Technol. A. 38 (2020), 023002, https://doi.org/10.1116/1.5132912.
[30] L. Bónová, A. Zahoranová, D. Kováčik, M. Zahoran, M. Mičušík, M. Černák, Atmospheric pressure plasma treatment of flat aluminum surface, Appl. Surf. Sci. 331 (2015) 79–86, https://doi.org/10.1016/j.apsusc.2015.01.030.
[31] Č.M. Bónová L., A. Buček, T. Plecenik, A. Zahoranová, Surface Treatment By Plasma Discharges and Thin Film Deposition Cleaning of Aluminium Surface Using Diffuse Coplanar Surface Barrier Discharge, Chem. List. 1454 (2008) 1452–1454.
[32] H. Li, A. Belkind, F. Jansen, Z. Orban, An in situ XPS study of oxygen plasma cleaning of aluminum surfaces, Surf. Coatings Technol. 92 (1997) 171–177, https://doi.org/10.1016/S0257-8972(97)00079-0.
[33] J. Muñoz, J.A. Bravo, M.D. Calzada, Aluminum metal surface cleaning and activation by atmospheric-pressure remote plasma, Appl. Surf. Sci. 407 (2017) 72–81, https://doi.org/10.1016/j.apsusc.2017.02.092.
[34] Z. Zhai, L. Feng, Effect of oxygen plasma treatment on bonding strength of epoxy coating on steel substrate, Prog. Org. Coatings. 131 (2019) 36–41, https://doi.org/10.1016/j.porgcoat.2019.02.011.
[35] C. Sun, J. Min, J. Lin, H. Wan, Effect of atmospheric pressure plasma treatment on adhesive bonding of carbon fiber reinforced polymer, Polymers (Basel) 11 (2019), https://doi.org/10.3390/polym11010139.
[36] E.M. Liston, Plasma treatment for improved bonding: A review, J. Adhes. 30 (1989) 199–218, https://doi.org/10.1080/00218468908048206.
[37] M. Noeske, J. Degenhardt, S. Strudthoff, U. Lommatzsch, Plasma jet treatment of five polymers at atmospheric pressure: Surface modifications and the relevance for adhesion, Int. J. Adhes. Adhes. 24 (2004) 171–177, https://doi.org/10.1016/j.ijadhadh.2003.09.006.
[38] R.M. Thurston, J.D. Clay, M.D. Schulte, Effect of atmospheric plasma treatment on polymer surface energy and adhesion, J. Plast. Film Sheeting. 23 (2007) 63–78, https://doi.org/10.1177/8756087907078698.
[39] J. Ge, A. Khanna, T. Mueller, Surface Passivation Using Silicon Oxide by Atmospheric Pressure Plasma Coating System, in: 2018 IEEE 7th World Conf. Photovolt. Energy Conversion, WCPEC 2018 - A Jt. Conf. 45th IEEE PVSC, 28th PVSEC 34th EU PVSEC, 2018, pp. 2129–2131, https://doi.org/10.1109/PVSC.2018.8547998.
[40] D. Merche, N. Vandencasteele, F. Reniers, Atmospheric plasmas for thin film deposition: A critical review, Thin Solid Films 520 (2012) 4219–4236, https://doi.org/10.1016/j.tsf.2012.01.026.